

Magnetotransport properties of a polarization-doped three-dimensional electron slab

Debdip Jena, Sten Heikman, James S. Speck, Arthur Gossard, and Umesh K. Mishra
 Department of Electrical and Computer Engineering and Materials Department
 University of California, Santa Barbara
 CA, 93106

Angela Link and Oliver Ambacher
 Walter Schottky Institute, Am Coulmbwall 3 D-85748 Garching, Germany
 (Dated: November 10, 2021)

We present evidence of strong Shubnikov-de-Haas magnetoresistance oscillations in a polarization-doped degenerate three-dimensional electron slab in an AlGaInN semiconductor system. The degenerate free carriers are generated by a novel technique by grading a polar alloy semiconductor with spatially changing polarization. A analysis of the magnetotransport data enables us to extract an effective mass of $m^* = 0.19m_0$ and a quantum scattering time of $\tau_q = 0.3\text{ps}$. A analysis of scattering processes helps us extract an alloy scattering parameter for the AlGaInN material system to be $V_0 = 1.8\text{eV}$.

PACS numbers: 81.10.Bk, 72.80.Ey

Keywords: polarization doping, three-dimensional electron slab (3DES), III-V nitride, Magnetoresistance, Shubnikov-de-Haas (SdH) oscillations, GaN, AlGaIn, effective mass, collision broadening, Dingle temperature, quantum scattering time, alloy scattering

I. INTRODUCTION

In a recent paper¹, we reported the creation of polarization-doped three-dimensional electron slabs (3DES) in a graded AlGaIn layer. In this work, we present magnetotransport studies of the polarization-doped 3DES. The 3DES exhibits strong Shubnikov-de-Haas oscillations. A study of these oscillations reveals the effective mass of carriers, the collisional broadening due to quantum scattering, and the nature of transport in the polarization-doped 3DES.

In a polar crystal with uniform composition, $n = r \cdot P = 0$ (where P is the polarization vector), and there is no bulk polarization charge. The polarization of the crystal manifests only as sheet charges at surfaces and interfaces, owing to the change in polarization across them ($\sigma = (P_1 - P_2) \cdot \hat{n}$, where σ is the sheet charge, P_1, P_2 are the polarization vectors on the two sides of the junction, and \hat{n} is the normal to the junction). An alloy of spatially constant composition of two polar materials with different magnitudes of polarization will also have $n = r \cdot P = 0$. However, if the composition changes spatially, the divergence of the polarization vector becomes non-vanishing. This leads to an immobile polarization charge $N^D = r \cdot P$ in a graded alloy region.

The III-V nitride family of crystals of the wurtzite crystal structure is among the first material systems that is strongly polar (compared to other III-V semiconductors) along the c -(0001) axis, is semiconducting (most strongly polar crystals are insulators and used as dielectrics), its binaries (GaN, AlN, InN) have different polarizations, and they can be grown epitaxially with sufficiently pure crystalline quality. These unique properties of the material system enables us to exploit the concept of polarization bulk doping. The large difference in polar-

ization between AlN and GaN (both spontaneous and piezoelectric)³ and the good control of epitaxial growth of AlGaIn alloys prompted its choice for this experiment.

Figure 1 shows a schematic of charge control and band diagram of the technique of polarization doping that we have employed. Also shown in the figure is the sample structure we have used. The sample is a Ga-face structure grown by plasma-induced molecular beam epitaxy⁵ on a metal-organic chemical vapor deposition grown semi-insulating⁶ GaN on a sapphire substrate. The growth is along the polar c (0001) axis⁴. The top 100nm of the structure is linearly graded AlGaIn; the composition of Al is changed from 0-30% by controlling the aluminum flux by a computer program¹. This is the layer that is polarization doped.

The linear grading leads to a fixed charge⁷ doping $N^D = r \cdot P$ terminated by a opposite sheet charge $\sigma = -P \cdot \hat{n}$ at the surface. The large electric field created by the junction of fixed polarization charge extracts electrons from surface donor states⁸ to form a mobile 3-dimensional electron slab (3DES). The mobile 3DES is characterized by a temperature independent carrier concentration for $0.4\text{K} < T < 300\text{K}$ verifying that the carriers are degenerate, and thus distinct from carriers activated from shallow donors¹. We now proceed to study the magnetotransport properties of the 3DES created by this novel process.

II. MAGNETOTRANSPORT

In the presence of a quantizing magnetic field, the unperturbed 3-dimensional density of states (DOS) $g_0(B)$ undergoes Landau quantization to quasi-1-dimensional density of states and acquires an oscillatory component. Dingle¹⁰ showed that inclusion of collisional broaden-

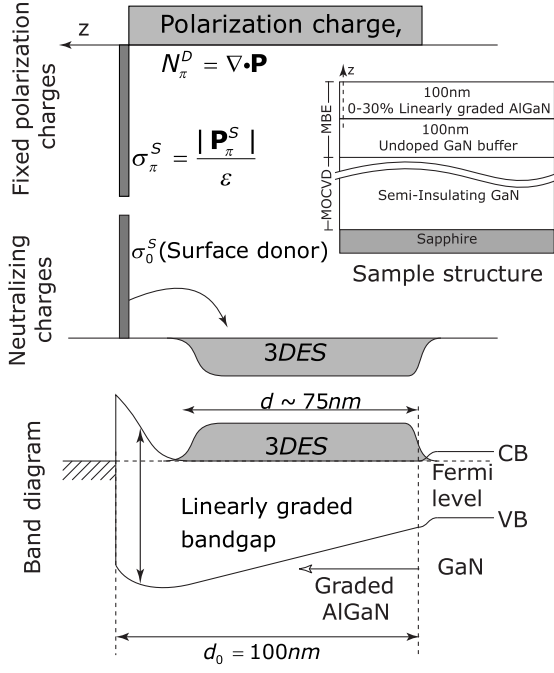


FIG. 1: Schematic of charge control showing polarization charges and formation of the 3DES. The band diagram shows depletion of the 3DES from the surface potential. Also shown is the epitaxial layer structure that generates the 3DES.

ing removes the divergence at the bottom of each 1-dimensional subband and damps the DOS oscillation amplitudes exponentially in $1/B$.

As is well known from the theory of the magnetic quantum effects, this oscillation of the density of states manifests in oscillations of both the diamagnetic susceptibility (manifesting in the de-Haas Van Alphen effect) and transport coefficients (manifesting in the Shubnikov de-Haas or SdH oscillations). In particular, the transverse ($B \perp E$) magnetoresistance R_{xx} shows oscillations in $1/B$. Kubo¹¹ derived the transverse magnetoresistance at high magnetic fields using the density-matrix approach to solve the transport problem. The expression for R_{xx} can be decomposed into a background part and an oscillatory contribution¹² $R_{xx} = R_{xx}^{\text{back}} + R_{xx}^{\text{osc}}$. The background term is attributed to sample inhomogeneities and disorder. The amplitude (A) of the oscillatory component can be cast in a form¹³ that is simple to use and captures the physical processes reflected in the measured magnetoresistance –

$$R_{xx}^{\text{osc}} / A = \frac{\sinh\left(\frac{2\pi^2 k_B T}{\hbar \omega_c}\right)}{\left(\frac{2\pi^2 k_B T}{\hbar \omega_c}\right)} \exp\left(-\frac{2\pi^2 k_B T}{\hbar \omega_c}\right) \left(\frac{\hbar \omega_c}{2\pi^2 k_B T}\right)^{1/2} \cos\left(\frac{2\pi^2 k_B T}{\hbar \omega_c}\right) \quad (1)$$

where R_{xx}^{osc} is the oscillating part of the magnetoresistance with the background removed, $\hbar \omega_c = (\hbar^2/2m^*) (3^2 n_{3DES})^{2/3}$ is the Fermi energy of the 3DES,

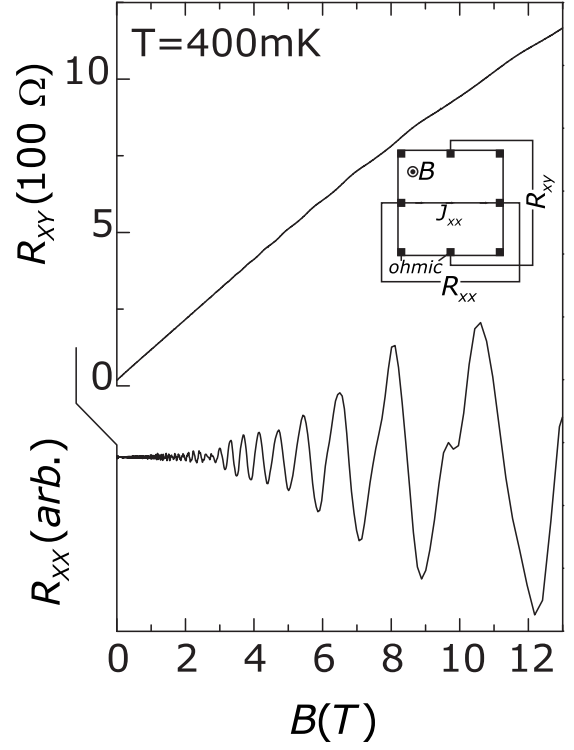


FIG. 2: Magnetotransport measurement data at $T = 400\text{mK}$. The figure also shown as an inset the geometry used for measuring R_{xx} ; R_{xy} . The R_{xx} shown is the oscillatory component with the background removed.

\sim being the reduced Planck's constant and n_{3DES} is the carrier density of the 3DES, and $\hbar \omega_c = eB/\hbar$ is the cyclotron frequency. $\hbar \omega_c / 2\pi^2 k_B T \sim \hbar \omega_c / k_B T$ is a temperature dependent dimensionless parameter and $\hbar \omega_c$ is the collisional broadening energy due to quantum scattering events. ϕ is a phase factor that is unimportant for our study. The terms $S_t(T)$ and $D_c(B)$ are the temperature and collision damping terms respectively; it is easily seen that in the absence of damping of the oscillations due to temperature ($\lim_{T \rightarrow 0} S_t(T) = 1$) and in the absence of damping due to collisions ($\lim_{B \rightarrow 0} D_c(B) = 1$), the magnetoresistance would exhibit a weakly modulated ($1/B^2$) cosine oscillations in $1/B$. In fact, the two damping terms $S_t(T)$; $D_c(B)$ are used as probes to tune the temperature and magnetic field independently to extract the effective mass and the quantum scattering time. The period of the cosine oscillatory term yields the carrier density of the 3DES since the period is linked to n_{3DES} . R_{xy} , the Hall resistance is linear with B , and should show plateaus at the minima of R_{xx} when a small number of Landau levels are filled.

For magnetotransport measurements on our 3DES, ohmic contacts were formed in a Van-der Pauw geometry (Figure 1 inset). The sample was immersed in a ^3He low-temperature cryostat with a base temperature of 300mK. Magnetic fields in the range 0T $\leq B \leq 14\text{T}$ were applied.

R_{xx} and R_{xy} was measured as in the geometry depicted in the figure using the standard low-frequency lock-in technique.

In Figure II we show a plot of the oscillatory transverse magnetoresistance R_{xx}^{osc} and R_{xy} at $T = 400\text{mK}$ plotted against the applied magnetic field. We have removed the background using a FFT filter for plotting R_{xx} . We will briefly describe our FFT process later in this work. The Hall mobility determined from the slope of the R_{xy} curve is $\mu_H \approx 3000\text{cm}^2/\text{Vs}$, which is higher than 77K low-field Hall mobility of $\mu_{77K} \approx 2500\text{cm}^2/\text{Vs}$. Also, assuming that the 3DES is spread over a thickness d , the sheet carrier density of the 3DES is calculated to be $n_{3DES} d = 1/R_H e = B/eR_{xy} = 7.2 \times 10^{12}/\text{cm}^2$. This is consistent with the 77K low-field Hall measured sheet density of $7.5 \times 10^{12}/\text{cm}^2$. The spread of the 3DES is calculated from a self-consistent Poisson-Schrodinger band calculation to be $d = 75\text{nm}$ due to 25nm depletion of the 3DES from the surface potential. This depletion in the graded AlGaIn layer has also been verified by capacitance-voltage profiling. Thus, the Hall 3-dimensional carrier density is $n_{3DES} = 10^{18}/\text{cm}^3$.

III. ANALYSIS OF MAGNETOTRANSPORT DATA

We begin our study by analyzing the oscillatory component of the transverse magnetoresistance (Figure III). For achieving this, we first take the raw R_{xx} vs B data and interpolate it to create an equally spaced $N = 2^{15}$ size FFT window. We then find the FFT power spectrum. This is repeated for R_{xx} measured at different temperatures. A typical FFT power spectrum (at $T = 2.5\text{K}$) is shown in the inset of Figure III. There is a clearly resolved peak at the fundamental oscillation period $B_0 = 34.01\text{T}$. A band pass filter [$f_{pass} = 28\text{--}150\text{T}$] is then employed to remove the background component. The resulting R_{xx}^{osc} for various temperatures $0.4\text{K} < T < 9.5\text{K}$ is plotted against $1/B$ in Figure III. As is clear from the plot, the period of oscillations is $(1/B) = 0.0294\text{T}^{-1} = 1/B_0$. The oscillations are strongly damped with increasing $1/B$ as well as with increasing temperature, as predicted by the theory (Equation 1).

A. Carrier concentration

First, we observe from Equation 1 that the period $(1/B)$ is linked to the carrier density of the 3DEG by the relation $(1/B) = e/\pi m^* \mu_F = \frac{2e}{\pi} (3^2 n_{3DES})^{-2/3}$. From the plot, the period $(1/B) = 0.0294\text{T}^{-1}$ yields a direct measurement of the 3-dimensional carrier concentration $n_{3D}^{SdH} = 1.1 \times 10^{18}/\text{cm}^3$. Thus, the carrier density measured from the quantum oscillations is close to the carrier density measured by classical Hall technique ($n_{3DES} = 10^{18}/\text{cm}^3$).

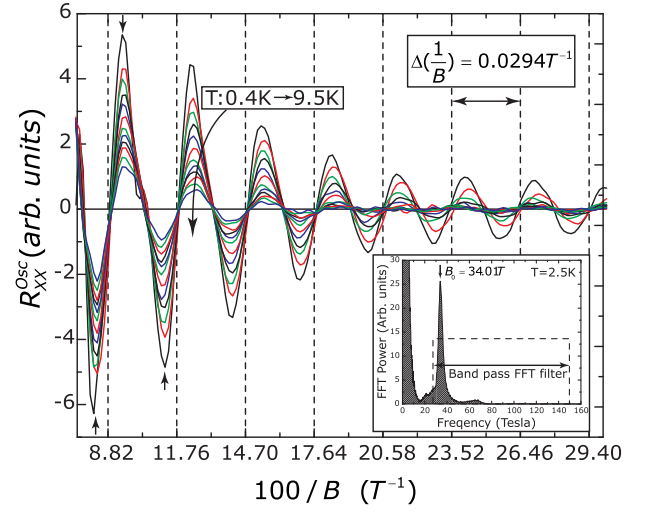


FIG. 3: The oscillatory component R_{xx}^{osc} plotted against $1/B$. The oscillations are periodic with period $(1/B) = 0.0294\text{T}^{-1}$, and are damped with both increasing temperature (different curves), and increasing $1/B$. Also shown in the inset is a typical FFT power spectrum (at $T = 2.5\text{K}$) showing a peak at the fundamental period, and the band-pass window used to filter the oscillatory component R_{xx}^{osc} .

B. Effective mass

The second important property of the 3DES that is accessible from the SdH oscillations is the effective mass of the electrons. This can be calculated from a controlled temperature damping of the oscillation amplitudes, i.e., by tuning the term $D_t(T)$ (which is the only temperature dependent term). The approximation $\sinh(x) \approx \exp(x)/2$ converts Equation 1 into

$$\ln\left(\frac{A}{T}\right) = C - \left(\frac{2^2 k_B m^*}{e\pi B}\right) T \quad (2)$$

where the constant C absorbs all terms independent of temperature. Thus, when $\ln(A/T)$ is plotted against T for a fixed magnetic field, it results in a straight line with slope $S = \frac{2^2 k_B m^*}{e\pi B}$. Since the effective mass is the only unknown, it can be calculated. We calculate the effective mass by employing this procedure.

We choose the amplitude maxima at three different magnetic fields $B = 8.9\text{T}; 10.5\text{T}; 12.0\text{T}$ for extracting effective mass of the 3DES. These maxima are indicated by arrows in Figure 3. The plots of $\ln(A/T)$ against temperature ($2.5\text{K} < T < 14.5\text{K}$) for these magnetic fields are shown in Figure IV (a). The slopes of the plots at $B = 8.9\text{T}; 10.5\text{T}; 12.0\text{T}$ yield effective masses $m^* = 0.189; 0.197; 0.189m_0$ respectively. The accepted effective mass of electrons in bulk GaN is $m^* = 0.2m_0$. SdH measurement of electron effective mass in bulk GaN is difficult since the activated carriers in donor-doped samples freeze out at low temperatures¹. Since the elec-

trons in our 3DES are degenerate, they resist freezeout effects and remain independent of temperature. However, the 3DES electron is not in bulk GaN but in an alloy with a changing composition; we expect the effective mass to be a spatial average. The effective mass of electrons in AlN is predicted¹⁴ to be $m^* = 0.32m_0$; a linear interpolation gives an expected effective mass of $m^* = 0.21m_0$ at an average alloy composition of $x = (0.75 - 0.3)/2 = 0.11$ for the mobile 3DES. This is slightly higher than our measured average value $m_{av}^* = 0.19m_0$. The result is reasonable within limits of experimental error. We also note that the effective mass of electrons in two-dimensional electron gases (2DEGs) at AlGaIn/GaN heterojunctions has been measured by SdH oscillation technique^{15,16,17,18} and reported to be various values around $m^* = 0.2m_0$, which is close to our measured value.

C. Scattering times

The third important parameter of the 3DES that is measured from the SdH oscillations is the collisional broadening energy (due to Dingle). This term is a measure of the smearing of the delta-function discontinuities in the DOS due to quantum scattering events, and it appears as the imaginary part of the single-particle self energy function. Collisional broadening energy is linked to the quantum scattering time τ_q and the Dingle temperature T_D by the relation $\Gamma = \hbar/2\tau_q = k_B T_D$. This quantity is experimentally accessible from a controlled Landau damping of the oscillation amplitudes with $1/B$ at a fixed temperature; in other words, by tuning $D_c(B)$. Equation 1 can be cast in the form

$$\ln \left(\frac{A^2}{(\frac{1}{2\pi})^{1/2} D_t(T)} \right) = C - \left(\frac{m^*}{e} \right) \frac{1}{B} \quad (3)$$

for extracting τ_q and the related quantities Γ ; T_D . Here A^2 are the extrema points of the damped oscillations, forming the exponentially decaying envelope. Equation 3 suggests that a plot of the natural log of the left side quantity against $1/B$ (Dingle plot) should result in a straight line whose slope is m^*/e . Since we have already measured the effective mass m^* , we can extract τ_q from the slope.

Figure IV (b) shows the Dingle plot for $T = 400$ mK, yielding a $\tau_q = 0.27$ ps. An averaging of the quantum scattering times over a range of low temperatures yields a value $\tau_q^{av} = 0.3$ ps. The quantum scattering time does not show any discernible trend with temperature in this range. We calculate the corresponding level broadening $\Gamma = 1.1$ meV and Dingle temperature $T_D = 4$ K. We mention in passing that the Landau level separation at $B = 10$ T is $\hbar\omega_c = 5.8$ meV, sufficiently larger than both the measured collisional broadening of the Landau levels ($\Gamma = 1.1$ meV) and the thermal broadening

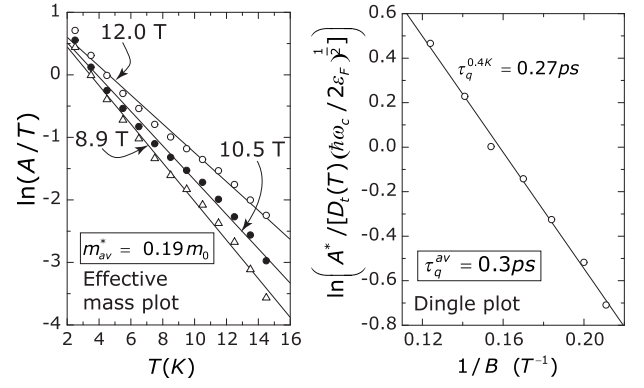


FIG. 4: Effective mass plot and Dingle plot of the 3DES. For effective mass, $\ln(A/T)$ is plotted for three values of magnetic fields ($B = 8.9$ T; 10.5 T; 12.0 T) against temperature. The slope yields the effective masses $0.189m_0$; $0.197m_0$; $0.189m_0$ respectively. The Dingle plot yields a quantum scattering time of $\tau_q = 0.27$ ps at $T = 400$ mK and an average value of $\tau_q^{av} = 0.3$ ps.

$k_B T = 0.09$ meV at $T = 1$ K, thus satisfying the conditions required for clear Shubnikov de-Haas oscillations.

Whilst τ_q (the quantum lifetime of an electron in a magnetic quantum state) is determined by all scattering events, the transport (classical, or momentum) lifetime τ_c is weighted by a scattering angle factor $(1 - \cos \theta)$, where θ is the angular deviation in the scattering event. Thus,

$$\frac{1}{\tau_q} = \int_0^\pi P(\theta) d\theta \quad (4)$$

as opposed to the momentum scattering time, which is averaged by the angular contribution for small angle scattering

$$\frac{1}{\tau_c} = \int_0^\pi P(\theta) (1 - \cos \theta) d\theta \quad (5)$$

here $P(\theta)$ is the transition probability between the initial and the scattered states determined by Fermi's golden rule. It can be seen that for isotropic scattering events with no angular preference ($P(\theta)$ is independent of θ), the quantum and classical scattering times are the same $\tau_c = \tau_q = 1$. If the dominant scattering process has a strong angle dependence, the ratio is much larger than unity. This fact has been utilized to identify the dominant scattering mechanism in modulation-doped AlGaAs/GaN two-dimensional electron gases¹⁹.

The low-temperature Hall mobility gives us a direct measurement of the classical scattering time for the 3DES via the relation $\mu_H = e\tau_c/m^*$; the value is $\tau_c = 0.34$ ps. Within limits of experimental error, the ratio $\tau_c = \tau_q = 1$, i.e., is close to unity.

D . Scattering mechanisms

As Hsu and Walukiewicz have shown²⁰, one has to exercise caution before declaring that the dominant scattering process in the 3DES is of short-range nature. They show that it is possible to have the ratio close to unity if there are different scattering mechanisms responsible for the quantum and classical lifetimes. At the low temperatures at which we measure the scattering time, both acoustic and optical phonon modes of scattering are frozen out and the charges from any unintentional background donors are frozen onto the donor sites, rendering them neutral. Size effect scattering²¹ that occurs if the width of the 3DES is much less than the mean-free path of electrons is negligible since our 3DES has a mean free path $\approx k_F \approx 60\text{nm}$ whereas the width of the 3DES is $d_0 \approx 75\text{nm}$. The chief scattering mechanisms that can affect mobility are alloy disorder scattering (since the 3DES is in a graded alloy), charged dislocation scattering (owing to the high density of dislocations $N_{\text{disl}} \approx 10^8\text{cm}^{-2}$), and ionized impurity scattering from the remote donors at the surface states.

Hsu and Walukiewicz²⁰ show that remote ionized impurity scattering strongly favors small angle scattering, thus causing the ratio $\mu_c/\mu_q \approx 1$. Since $\mu_c/\mu_q \approx 1$ for our 3DES, remote ionized impurity scattering is unimportant.

The ratio of classical to quantum scattering times due to charged dislocation scattering has not been found yet. Look²² recently applied the classical scattering time due to charged dislocations and applied it to explain the mobility of bulk doped GaN samples. The ratio classical to quantum scattering times due to charged dislocation scattering in a degenerate 3DES is given by²⁴

$$\frac{\tau_{\text{disl}}}{\tau_q} = 1 + 2k_F^2 \frac{\tau_F}{\tau_{\text{disl}}} \quad (6)$$

where $k_F = (3/2 n_{3\text{DES}})^{1/3}$ is the Fermi wavevector and $\tau_F = 2/\nu_F = 2/(3e^2 n_{3\text{DES}})$ is the Thomas-Fermi screening length for a degenerate 3DES. The ratio, which depends only on the 3D carrier density for a degenerate 3DES, is evidently greater than unity; for our 3DES, the ratio is 2.3, which is larger than what we observe. So dislocation scattering is not the dominant scattering mechanism for determining the quantum scattering rate. The dislocation scattering dominated classical scattering rates is strongly dependent on the amount of charge in the dislocation cores, which is low for our 3DES due to the lack of shallow dopants²³. Thus, we exclude dislocation scattering to be the most important scattering mechanism for classical scattering rate.

So we converge on alloy scattering as the dominant scattering mechanism for low temperatures. The quantum and classical scattering rates for alloy disorder scattering are the same since the scattering potential V_0 is of a short range nature, which makes the scattering process angle independent.

The scattering rate due to alloy disorder with a short range potential V_0 has been shown¹³ to be given by

$$\frac{1}{\tau_{\text{alloy}}(k)} = \frac{2}{\pi} V_0^2 \langle x \rangle x (1 - x) g_D(\epsilon_k) \quad (7)$$

where $\langle x \rangle$ is alloy composition-dependent volume of the unit cell over which the alloy scattering potential V_0 is effective, and x is the alloy composition. $g_D(\epsilon)$ is the 3-dimensional DOS. Since the 3DES is highly degenerate, only carriers with wavevectors very close to $k = k_F$ contribute to transport at low temperatures; hence, the scattering rate is evaluated at the Fermi energy $\frac{1}{\tau_{\text{alloy}}} = \frac{1}{\tau_{\text{alloy}}}(\epsilon_F)$. Besides, the alloy is graded, and Matthiessen's rule which is accurate for low temperature transport analysis is used for a spatial averaging of the scattering rate

$$\frac{1}{\tau_{\text{alloy}}} = \frac{1}{x_0} \int_0^{x_0} \frac{1}{\tau_{\text{alloy}}(x)} dx \quad (8)$$

where $x_0 = 0.225$ is the alloy composition experienced by 3DES electrons at the edge of the depletion region. Using this simple result, we conclude that to achieve a low-temperature transport mobility of $3000\text{cm}^2/\text{Vs}$, an alloy scattering potential of $V_0 = 1.8\text{eV}$ is necessary.

It is important to point out that the alloy scattering potential as defined in the model for alloy disorder is at best a fitting parameter. Due to the lack of experimental values, it is common practice to assume the scattering potential to be the conduction band offset between the binaries forming the alloy ($V_0 = E_c = 2.1\text{eV}$ for AlN/GaN). We note that with an alloy scattering potential of $V_0 = 2.1\text{eV}$, the calculated mobility is lower ($\approx 2000\text{cm}^2/\text{Vs}$) than the measured value. Besides, our 3DES mobility is dominated by alloy scattering and all other scattering mechanisms are removed by measuring the mobility at low temperatures, making it a clean measurement of the alloy scattering potential. Our report presents the first direct measurement of the alloy scattering potential in the AlGaN material system.

IV . SUMMARY

We finally summarize our findings in this work (see Table I). By exploiting the polarization charges in the Al-GaN/GaN semiconductor system, we are able to create a 3DES without intentional doping. The mobile carriers in the 3DES are degenerate and exhibit a high mobility even to the lowest temperatures. The lack of carrier freezeout enables us to observe Shubnikov-deHaas oscillations in magnetotransport measurements of the 3DES. The oscillations reveal several important facts about the 3DES. First, the temperature damping of oscillations reveals the effective mass of electrons to be very close to that in bulk GaN ($m^* = 0.19m_0$). Next, the quantum

scattering time of electrons in the 3DES is found from the Dingle plot to be $\tau_q = 0.3$ ps. The ratio of the classical (momentum) scattering time to the classical (momentum) scattering time is found to be close to unity $\tau_c = \tau_q = 1$. The ratio suggests predominantly short-range scattering dominating transport properties at low temperatures. This scattering mechanism is identified to be alloy scattering. This lets us extract another valuable parameter, the alloy scattering potential in $\text{Al}_x\text{Ga}_{1-x}\text{N}$ to be $V_0 = 1.8\text{eV}$.

Acknowledgments

The authors would like to thank Jasprit Singh, and Herbert Kroemer for useful discussions, and Huili Xing for a critical reading of the manuscript. Funding from POLARIS/MURI (Contract monitor: C. Wood) is gratefully acknowledged.

Electronic mail: djena@engineering.ucsb.edu

- ¹ D. Jena et. al, Accepted for publication in Appl. Phys. Lett.
- ² L. Pfeiffer, K. W. West, H. L. Stormer and K. W. Baldwin, Appl. Phys. Lett. 55, 1888 (1989).
- ³ F. Bernardini, V. Fiorentini, and D. Vanderbilt, Phys. Rev. B 56, R10 024 (1997).
- ⁴ P. Waltereit et. al, Nature 406, 865 (2000).
- ⁵ B. Heying, R. Averbeck, L. F. Chen, E. Haus, H. Riechert, and J. S. Speck, J. Appl. Phys., 88 1855 (2000)
- ⁶ S. Heikman, S. Keller, S. P. DenBaars, and U. K. Mishra, Appl. Phys. Lett., 81 439 (2002)
- ⁷ There is a small nonlinearity associated with the piezoelectric component which can be neglected.
- ⁸ J. P. Ibbetson et. al, Appl. Phys. Lett. 77, 250 (2000).
- ⁹ M. Shayegan, T. Sajto, M. Santos, and C. Silvestre, Appl. Phys. Lett. 53, 791 (1988)
- ¹⁰ R. B. Dingle, Proc. Roy. Soc. A 211, 517 (1952).
- ¹¹ R. Kubo, H. Hasegawa, and N. Hashitsume, J. Phys. Soc. Japan 14, 56 (1959).
- ¹² L. M. Roth and P. M. Agyres, Semiconductors and Semimetals 1, 159 (1966).
- ¹³ C. Hamaguchi, Basic Semiconductor Physics, 280 (2001).
- ¹⁴ I. Vurgaftman, J. R. Meyer and L. R. Ram-Mohan, J. Appl. Phys., 89 8815 (2001)
- ¹⁵ S. Elhamriet et. al Phys. Rev. B 57, 1374 (1998).
- ¹⁶ W. Knap et. al Appl. Phys. Lett. 70, 2123 (1997).
- ¹⁷ A. Saxler et. al J. Appl. Phys. 87, 369 (2000).
- ¹⁸ Z. W. Zheng et. al Phys. Rev. B 62, R7739 (2000).
- ¹⁹ J. P. Harrang, R. J. Higgins, R. K. Goodall, P. R. Ray, M. Laviron, and P. D. Eaglescluse, Phys. Rev. B., 32, 8126 (1985).
- ²⁰ L. Hsu and W. Walukiewicz, Appl. Phys. Lett. 80, 2508 (2002).
- ²¹ W. Walukiewicz, P. F. Hopkins, M. Sundaram, and A. C. Gossard, Phys. Rev. B., 44, 10909 (1991).
- ²² D. C. Look and J. R. Sizelove, Phys. Rev. Lett., 82, 1237 (1999)
- ²³ K. Leung, A. F. Wright, and E. B. Stechel, Appl. Phys. Lett., 74, 2495, (1999)
- ²⁴ D. Jena and U. K. Mishra, cond-mat/0209663.

TABLE I: Summary of constants used and results extracted from magnetoresistance measurements

| Quantity | Symbol | Magnitude | Unit |
|------------------------------|--------------|--------------------------|-------------------------|
| Relative dielectric constant | ϵ_r | 8.9 (GaN), 8.5 (AlN) | — |
| Lattice constant | a_0 | 3.189 (GaN), 3.112 (AlN) | Å |
| Lattice constant | c_0 | 5.185 (GaN), 4.982 (AlN) | Å |
| Effective mass | m^* | 0.19 | m_0 |
| Quantum scattering time | τ_q | 0.3 | ps |
| Transport scattering time | τ_m | 0.34 | ps |
| 3DES density | n_{3DES} | $1.1 \cdot 10^{18}$ | cm^{-3} |
| 3DES Hall mobility (1K) | μ_H | 3000 | cm^2/Vs |
| Alloy scattering potential | V_0 | 1.8 | eV |